

Reinforcement learning for optimal error correction of toric codes

Laija Domingo Colomer, Michalis Skotiniotis, and Ramon Muñoz-Tapia
*Física Teòrica: Informació i Fenòmens Quàntics, Departament de Física,
Universitat Autònoma de Barcelona, 08193 Bellaterra (Barcelona) Spain*
(Dated: February 24, 2020)

We apply deep reinforcement learning techniques to design high threshold decoders for the toric code under uncorrelated noise. By rewarding the agent only if the decoding procedure preserves the logical states of the toric code, and using deep convolutional networks for the training phase of the agent, we observe near-optimal performance for uncorrelated noise around the theoretically optimal threshold of 11%. We observe that, by and large, the agent implements a policy similar to that of minimum weight perfect matchings even though no bias towards any policy is given *a priori*.

I. INTRODUCTION

Computation using quantum mechanical systems holds much promise as the ability of quantum systems to exist in exotic states, such as quantum entanglement and superposition, is known to yield significant advantages in computation [1, 2], communication [3], and sensing [4, 5]. Due to the fragility of such exotic states to environmental decoherence, the ability to actively protect sensitive quantum information against noise by quantum error correction [6, 7] is indispensable on the road to a fully fault-tolerant quantum computing infrastructure [8]. Quantum error correcting codes (QECC) need to be efficiently implementable both in terms of the physical operations as well as the time needed to recover corrupted quantum data. A promising platform are topological error correcting codes (TECC) [9, 10] for which the recovery operations consist of quasi-local error-syndrome measurements and local Pauli correction operations. A drawback of QECC, and TECC is that the error configuration space grows prohibitively large with the number of errors, and error syndromes exhibit high degeneracy making the design of optimal, fast decoders a highly non-trivial task.

In recent years several approaches based on cellular-automata [11–14], renormalization group [15, 16], restricted Boltzman machines [17], and machine learning [18–27] have produced a plethora of high performance QECC and TECC decoders. Particularly for TECC decoders designed using these techniques have shown to achieve similar performance to the best known decoder based on the minimum weight perfect matchings (MWPM) algorithm [28]. Specifically, [17] used a stochastic neural network in a supervised learning paradigm to design decoders for the toric code under phase flip noise, whereas [19] used deep neural networks to design decoders that outperform MWPM for surface codes in the case of correlated noise. Baireuther *et al.* [20] used a recurrent neural network, trained only on experimental data, to decode a surface code under correlated noise with high accuracy, whereas [18] used feedforward neural networks to construct fast, but not necessarily optimal, decoders for surface codes. Shortly after the same authors showed that a combination of renormalization techniques with neural networks is ca-

pable of providing fast, high threshold decoders [25]. Feedforward neural networks were also used to construct high threshold decoders for the toric and color codes under several noise models, including spatially correlated noise [26].

In the above machine learning approaches the training is performed in a supervised manner. A more general framework of machine learning is reinforcement learning (RL) where the agent is unsupervised and learns by simply interacting with its immediate environment and receiving feedback in terms of rewards. Sweke *et al.* combined RL with deep Q learning (DQL) to design fast decoders for the surface code under correlated noise and noisy syndrome measurements, whereas in [27] RL and DQL were used to design high threshold decoders for the toric code under phase flip noise. It is worth noting that machine learning techniques have also been used for optimally designing the requisite QEC [21, 29, 30].

Here we construct model-free optimal decoders for the toric code in the presence of uncorrelated noise. Just as in [27], we use deep convolutional networks and episodic memory to train an agent in a RL paradigm but employ a fundamentally different system of rewards. In [27] agents were rewarded based on the number of actions taken, not whether the resulting actions yielded a successful decoding procedure. Indeed, the authors state that whilst the latter reward system is more natural, they found it difficult to train their agents using it. We show that agents can be trained within a few hours using rewards based solely on the correct decoding of the quantum information and show that our decoders reach near optimal performance just shy of the optimal threshold. Our decoders exhibit good performance even when trained with error rates slightly above percolation. We compare our agents performance to those of [27] by comparing their respective episode lengths and find them to be nearly identical thus further supporting the intuition that the optimal decoders are those that take the minimum number of actions in order to correct the syndrome.

The article is structured as follows. In Sec. II we briefly review the principles of QECC and the stabiliser formalism and introduce TECC and in particular the toric code. In Sec. III we introduce the interaction-

based learning scenario between an agent and an environment and give a basic review of reinforcement learning and its implementation. In Sec. IV we formulate the decoding of the toric code in the presence of uncorrelated noise as a reinforcement learning problem and present the results of applying such decoders of up to 9×9 lattices. We summarize and conclude in Sec. V.

II. QUANTUM ERROR-CORRECTION AND THE TORIC CODE

Quantum information deals with the storage, transmission and manipulation of information represented in the states of quantum mechanical systems. Unfortunately, quantum systems are notoriously sensitive to the effects of noise which implies that their information depletes fairly quickly. A way to counteract the deleterious effects of noise is to make use of quantum error correcting codes (QECC) (see [31] and references therein). Much like classical error correction the idea behind QECC is to use a number, n , of *physical* quantum systems, each with an associated state space \mathcal{H} , and identify a suitable subspace, $\mathcal{C} \subset \mathcal{H}^{\otimes n}$, onto which quantum information can be protected by decoherence. A crucial ingredient in QECC are the encoding and decoding operations to and from the *code space* \mathcal{C} . Ideally we seek to design codes with large error tolerance, high storage capacity, and efficient encoding, decoding and recovery operations. Hereafter, all physical systems we consider are two-dimensional quantum systems (qubits).

The dimension, d , of the code space, \mathcal{C} , defines the number of distinct *logical* states, or codewords, as well as the number of *logical* qubits, $k = \log_2 d$. The *distance*, δ , of a code is the number of errors it can correct. By way of example, the three-qubit repetition code utilizes the code space $\mathcal{C} := \text{span}\{|0\rangle_L \equiv |000\rangle, |1\rangle_L \equiv |111\rangle\}$, of three physical qubits to store one logical qubit and protect it against a single qubit X error. Here we denote by

$$X = \begin{pmatrix} 0 & 1 \\ 1 & 0 \end{pmatrix}, \quad Y = \begin{pmatrix} 0 & -i \\ i & 0 \end{pmatrix}, \quad Z = \begin{pmatrix} 1 & 0 \\ 0 & -1 \end{pmatrix}, \quad (1)$$

the usual Pauli matrices.

As the number of physical qubits and error thresholds for QECC grows working directly with logical states and their superpositions becomes inefficient. Thankfully, an efficient description of QECCs exists in terms of the stabilizer formalism [32, 33]. A subspace $\mathcal{C} \subset \mathcal{H}^{\otimes M}$ is said to be *stabilized* by an operator $P \in \mathcal{B}(\mathcal{H}^{\otimes M})$ if for any $|\psi\rangle \in \mathcal{C}$, $P|\psi\rangle = |\psi\rangle$. If this is the case then P is called a *stabilizer* of the code and \mathcal{C} is uniquely specified as the eigenspace of the complete set of commuting stabilizers $\mathcal{P} := \{P_i, i \in (1, \dots, N) \mid [P_i, P_j] = 0, \forall i \neq j\}$ with eigenvalue +1. Note that \mathcal{P} forms a finite Abelian group under matrix multiplication and consequently can be generated by $m = \log_2 N$ suitably chosen generators.

The number of generators m , logical qubits k , and physical qubits n are related by $m = n - k$.

In order to encode logical quantum information we need to construct the logical Pauli operators, X_L, Z_L in such a way that they commute with the stabiliser group \mathcal{P} . For the three-qubit code, we have

$$\mathcal{P} = \{Z \otimes Z \otimes \mathbf{1}, \quad Z \otimes \mathbf{1} \otimes Z, \quad \mathbf{1} \otimes Z \otimes Z, \quad \mathbf{1} \otimes \mathbf{1} \otimes \mathbf{1}\}, \quad (2)$$

and one can easily check that the following operators

$$X_L = X \otimes X \otimes X \quad Z_L = Z \otimes \mathbf{1} \otimes \mathbf{1}, \quad (3)$$

commute with those of Eq. (2), and satisfy the Pauli commutation relations.

Decoding, on the other hand, is a two-stage process involving first a recovery operation before extracting the relevant quantum information. The recovery operation consists of measuring all 2^m stabilizers and, based on the measurement outcomes—the *error syndrome*—apply Pauli correction operations on the n physical qubits. If the syndrome contains all +1 then no recovery operation is required, whereas -1 values in the syndrome indicate the presence of errors. For the three-qubit code, $m = 3 - 1 = 2$. The error syndromes of $Z \otimes Z \otimes \mathbf{1}$ and $\mathbf{1} \otimes Z \otimes Z$ uniquely identify the physical qubit on which a Pauli X error occurred. Note, however, that in general the relationship between physical errors and the syndrome read-out is not unique. There may be many error configurations which lead to the same syndrome, a phenomenon that occurs frequently in topological QECC which we now review.

Topological QECC: the toric code

Constructing QECC with high capacity for quantum information and large distance poses a serious challenge as both stabilizers and logical operations are generally *global* operators acting on all n physical qubits. An alternative, and more resource intensive, way of constructing QECCs is to exploit the topological properties of multi-qubit systems arranged on a lattice [9, 10]. Such topological error correcting codes attain superb protection from decoherence, while requiring only local gates for error-correction and have been experimentally constructed in a variety of architectures [34–40]. In the remainder of this work, we shall focus on one of the simplest TECC, the toric code [9].

The toric code defined over an $d \times d$ square lattice, consists of $n = 2d^2$ physical qubits placed on every edge of the lattice. The topology of the torus arises from two distinct boundary conditions, one for the left and right edge of the lattice and one for the top and bottom edges. The stabilizer group of the toric code is generated by two distinct stabilizers associated with the plaquettes and vertices of the lattice (see Fig. 1(a)). Specifically, to every plaquette, p , and vertex v , the operators

$$P_p = \bigotimes_{j \in \text{boundary}(p)} Z_j, \quad Q_v = \bigotimes_{j \in \text{vertex}(v)} X_j \quad (4)$$

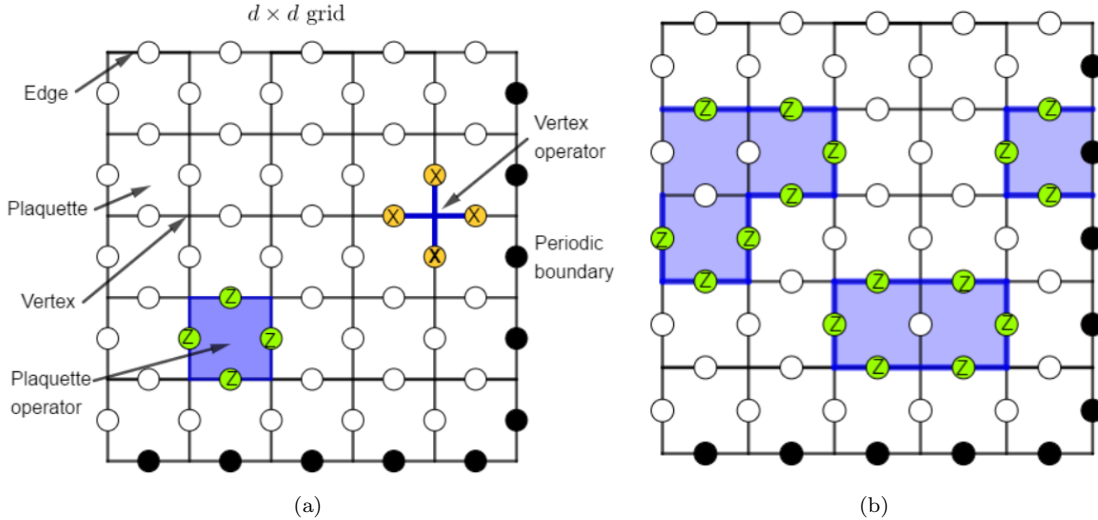


FIG. 1. The basic ingredients of the toric code: (a) A 5×5 lattice with the topology of a torus. The right and left boundaries of the lattice satisfy one periodic boundary condition, whereas the top and bottom edges the other periodic boundary condition. Physical qubits—represented as circles—are placed on the edges of the lattice. The stabilizers of the toric code are associated with *plaquette* operators (shaded blue square), and *vertex* operators (dark blue star) (b) Examples of multiplication of plaquette operators. The resultant operator consists of Z operators acting on the boundary of the combined plaquettes, and correspond to a stabilizer operator.

are stabilizers of the toric code, and there are a total of $2(d^2 - 1)$ independent plaquette and vertex operators forming the generators of its stabilizer group. Observe that adjacent plaquette and vertex operators commute as they overlap on exactly two physical qubits. Products of plaquette (vertex) operators are also stabilizers of the torus and give rise to *trivial loops* as illustrated in Fig. 1(b).

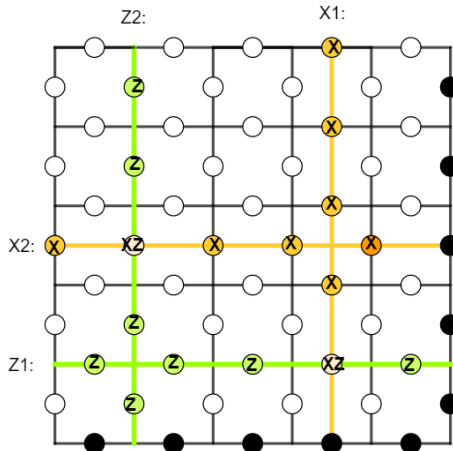


FIG. 2. The logical Pauli operators $\{X_L^{(i)}, Z_L^{(i)}\}_{i=1}^2$.

The dimension of the code space is $2d^2 - 2(d^2 - 1) = 2$. The logical operators, $\{X_L^{(i)}, Z_L^{(i)}\}_{i=1}^2$, for each of the logical qubits are shown in Fig. 2. They form *non-trivial* closed loops around the torus with $Z_L^{(1)}$ forming horizontal loops, $Z_L^{(2)}$ vertical loops and the correspond-

ing $X_L^{(i)}$ being closed loops orthogonal to those of $Z_L^{(i)}$. Notice, however, that the construction of the logical operators is not unique: we can generate an equivalence class of logical operators, acting identically on the code space, by multiplying the above logical operators with elements of \mathcal{P} (i.e., the loops do not need to be straight).

From the preceding discussion it follows that for a logical error to occur, an odd number of non-trivial loops around the torus must occur. Therefore, the distance of the toric code is d . If a physical qubit suffers an error, the stabilizer generators adjacent to the position of the physical qubit will have error syndrome -1 . However, the error syndrome distribution is never one to one with the physical errors of the lattice. There can be many different combinations of physical errors which lead to the same error syndrome, as shown in Fig. 3. Therefore, smart strategies are needed to return the faulty state to the initial logical state. The agent must perform physical operations which do not result in non-trivial loops around the torus, and thus logical errors, whilst returning the state to the codespace.

In addition, the design of optimal decoders also relies heavily on the types of errors occurring as well as their distribution. The simplest and most common noise models assume that each qubit experiences an independent and identically distributed (i.i.d.) noise process, with a probability p of suffering an error. Among the uncorrelated noise models, the most relevant ones are bit-flip (X errors) and phase-flip (Z errors) errors. For *correlated errors*, depolarizing noise (X, Y, Z noise each with probability $p/3$) is the most paradigmatic noise model. In this work we shall only consider uncorrelated noise and without loss of generality we shall assume bit-

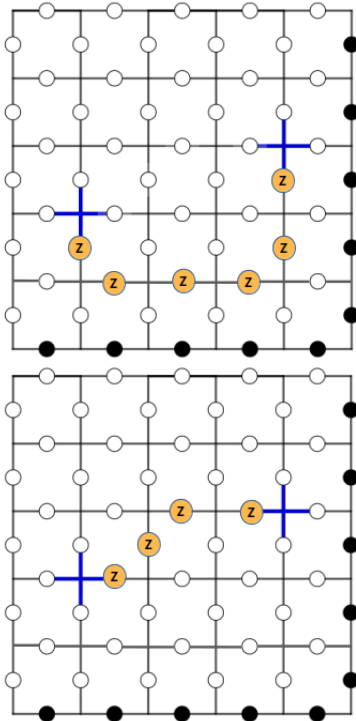


FIG. 3. Example of different physical errors (orange circles) leading to the same vertex syndrome error (blue lines crossing a vertex).

flip noise (analysis for phase-flip errors is completely analogous). Correlated noise is more challenging and will be addressed in future work. The optimal threshold of a decoder, on the other hand, is the maximum value of p for which recovery of the information is possible. For the toric code under i.i.d bit-flip errors this threshold is known to be 11% [41].

A widely used decoder for the toric code under bit-flip errors is based on the minimum weight perfect matchings (MWPM) algorithm [42, 43]. MWPM adopts the policy of correcting for the most likely error given a particular error syndrome and has proven to be a very successful decoder with an estimated threshold of 10.3% [44]. Recently, machine learning techniques and applications of (deep) neural networks have been applied in search for optimal decoders, both for topological as well as standard QECC [18–25, 27]. We now review the main techniques in reinforcement learning which we will use in search of efficient decoders for the toric code.

III. REINFORCEMENT LEARNING

Reinforcement learning (RL) is a framework within which one can precisely formulate the old dictum of “learning through experience” [45]. Agents trained using RL have excelled at performing certain tasks, such as mastering the game of Go [46], better than humans and RL based agents are used exten-

sively in robotics [47], artificial intelligence [48], and face-recognition [49]. Here we introduce the agent-environment paradigm of RL and review its key features; state and state-action valued functions. We then briefly discuss deep Q-learning (DQL) which uses deep convolutional networks highlighting some key techniques used to guarantee convergence in the training process for the agent.

Consider a scenario involving an agent, A , sequentially interacting with its immediate environment, E , in order to learn how to achieve a specific task (see Fig. 4). Here, learning is to be understood as A ’s ability to refine its future behaviour based on past experience in order to maximise future reward. Regardless of the details of A , E , and their interaction any such learning scenario can be modelled using the following three ingredients [45]: the set of all possible states, \mathcal{S} , of E , the set of all possible actions, \mathcal{A} , of A , and the set of rewards, \mathcal{R} —an assessment of A ’s performance towards the task. If the interaction is known, then one talks of *model-based* RL, otherwise the latter is *model-free*.

The learning process of A can be described in terms of *episodes* [50]. A and E interact, as shown in Fig. 4, and the episode finishes when the agent reaches the terminal state. Any given step $k \in \mathbb{Z}_N$ in an episode consists of A receiving the reward $r_k \in \mathcal{R}$ —from her/his previous action—and the current state of E , $s_k \in \mathcal{S}$. A then performs action $a_k \in \mathcal{A}$, after which E sends reward $r_{k+1} \in \mathcal{R}$, and its state changes to $s_{k+1} \equiv \mathcal{E}_k(s_k) \in \mathcal{S}$. Here boldface subscripts for the actions and state changes to the state of the environment indicate that these may depend on the history of actions and past states of the environment.

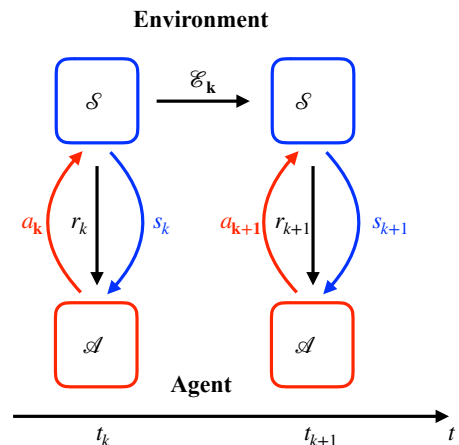


FIG. 4. A step in an episode in a general RL problem. The agent receives reward r_k from her/his previous action while the current state of the environment is $s_k \in \mathcal{S}$. The agent performs action $a_k \in \mathcal{A}$ which causes the environment to update its state to $s_{k+1} = \mathcal{E}_k(s_k)$, and reward the agent with $r_{k+1} \in \mathcal{R}$. This interaction is repeated until a terminal state $s_T \in \mathcal{S}$ is reached, and the episode finishes. The sequence $\{(r_k, s_k, a_k)\}_{k=1}^T$ within the episode is called a *trajectory*.

The set of states, rewards, and actions of an episode

are random variables, and the interaction between A and E is a stochastic map $\mathcal{E}_{\mathbf{k}} : \mathcal{S} \rightarrow \mathcal{S}$, that may depend on all preceding states of E and actions of A . Specifically, the probability that A receives reward r_{k+1} , and the state of E at step $k+1$ is s_{k+1} , given all preceding states $s_{\mathbf{k}} = s_1 s_2 \dots s_k$ and actions $a_{\mathbf{k}} = a_1 a_2 \dots a_k$ is $p(s_{k+1}, r_{k+1} | s_{\mathbf{k}}, a_{\mathbf{k}})$. If the conditional probabilities depend solely on the last preceding state of E and action of A , i.e., $p(s_{k+1}, r_{k+1} | s_{\mathbf{k}}, a_{\mathbf{k}}) = p(s_{k+1}, r_{k+1} | s_k, a_k)$, $\forall s_{k+1}, s_k, r_{k+1}$, and a_k then every finite sequence of steps is formally equivalent to a finite Markov decision process (MDP) [51]. The average reward an agent A expects to obtain after performing action a_k , given the state of the environment is s_k , is then

$$\mathbb{E}[r_{k+1}(s_k, a_k)] = \sum_{r_{k+1} \in \mathcal{R}} r_{k+1} \sum_{s_{k+1} \in \mathcal{S}} p(s_{k+1}, r_{k+1} | s_k, a_k). \quad (5)$$

Note that whilst we have assumed that both state and action spaces are finite dimensional, Eq. (5) can be equally applied to infinite dimensional cases.

The learning of the agent is quantified by the *expected discounted return*

$$R_k := \sum_{n=0}^T \gamma^n r_{k+n+1}, \quad (6)$$

where $0 \leq \gamma \leq 1$ is the *discount rate* [52]; $\gamma = 0$ favours only immediate rewards, and for $0 < \gamma < 1$, larger values of γ give more importance to long-term rewards than smaller values of γ . In the limit, when $\gamma = 1$, all rewards are given the same value. The decision making process of A is known as a *policy* and consists of a complete specification of the actions A will perform at every step of the sequence and for any possible state of E . Given a state s_k the probability that A will perform action a_k is denoted by $\pi(a_k | s_k)$. Under a policy π the value of a state s_k , $v_{\pi}(s_k)$, quantifies its average expected future returns, i.e., $v_{\pi}(s_k) = \mathbb{E}[R_k | s_k]_{\pi(A|s_k)}$. Similarly, the value of an action a_k given a state s_k —known as the *q-value* $q_{\pi}(s_k, a_k)$ —quantifies the average expected future returns of that action, i.e., $q_{\pi}(s_k, a_k) = \mathbb{E}[R_k | s_k, a_k]_{\pi(A, a_k | \mathcal{S}, s_k)}$. Such policy-value functions induce a partial order in the space of all possible policies of an agent: π is at least as good as π' , if and only if $v_{\pi}(s_k) \geq v_{\pi'}(s_k)$, $\forall s_k \in \mathcal{S}$. A policy π^* is optimal if no other policy can give a higher value than it, $v_{\pi^*}(s_k) = \max_{\pi} v_{\pi}(s_k)$ [45].

To determine the optimal policy one makes use of the recursive nature of both $v_{\pi}(s_k)$, and $q_{\pi}(s_k, a_k)$ to write

$$\begin{aligned} v_{\pi}(s_k) &= \sum_{a_k \in \mathcal{A}} \pi(a_k | s_k) \sum_{s_{k+1}} \sum_{r_{k+1}} p(s_{k+1}, r_{k+1} | s_k, a_k) \\ &\quad \times (r_{k+1} + \gamma v_{\pi}(s_{k+1})) \\ &= \sum_{a_k \in \mathcal{A}} \pi(a_k | s_k) \mathbb{E}[r_{k+1}(s_k, a_k)] + \gamma v_{\pi}(s_{k+1}) \end{aligned} \quad (7)$$

and

$$q_{\pi}(s_k, a_k) = \mathbb{E}[r_{k+1}(s_k, a_k)] + \gamma q_{\pi}(s_{k+1}, a_{k+1}). \quad (8)$$

Eqs. (7), and (8) are known as the *Bellman equations* [53] for state and state-action-value functions. For the optimal policy π^* , $v_{\pi^*}(s_k)$ takes the specific form

$$\begin{aligned} v_{\pi^*}(s_k) &= \max_{a_k \in \mathcal{A}} \sum_{s_{k+1}} \sum_{r_{k+1}} p(s_{k+1}, r_{k+1} | s_k, a_k) \\ &\quad \times (r_{k+1} + \gamma v_{\pi^*}(s_{k+1})) \end{aligned} \quad (9)$$

known as the Bellman optimality equation. Note that an optimal policy is known to always exist, though it may not be unique [54].

Agent training: Deep Q-learning

If the environment in a MDP is known then the optimal policy can be obtained by solving $|\mathcal{S}|$ Bellman equations. For model-free RL no such possibility exists and consequently state and state-action-value functions need to be estimated from experience. A typical algorithm used in this case is called *Q-learning*, with guaranteed convergence to the optimal q -value if every state-action pair is observed a sufficiently large number of times, i.e., if the agent is trained infinitely long [45]. For large state spaces this is prohibitively expensive. Consequently we have to resort to finite training sets which in turn means that the agent will often encounter situations previously unseen.

Deep Q-learning (DQL) uses deep convolutional networks [55], specialised for processing high-dimensional data, in order to extract global features and patterns. Upon encountering a previously unseen state, DQL uses such global features to compare with similar situations in past experience [56]. DQL parametrises the q -function in terms of a neural network, so that given an input state and action, the neural network produces the q -value $q(s, a)$ as an output. During training, the network parameters are adjusted, via stochastic gradient descent, such as to reduce the error between the optimal and approximated target q -values.

We use DQL to train our agent to successfully decode uncorrelated bit or phase flip noise on the toric code. Training halts either after a certain number of episodes have happened, or until the loss function of the convolutional neural network stops decreasing. To ensure stability during training we also make use of additional training techniques, such as double deep Q-learning, duelling deep Q-learning, and prioritised experience replay [57, 58].

IV. DEEP RL DECODERS FOR UNCORRELATED NOISE

We now cast decoders for the toric code under uncorrelated noise as a RL problem and present the results of

training model-free agents to accomplish the task. As already mentioned we discuss only the case of bit-flip errors. The environment, E , consists of the state of the toric code; a matrix of $2d^2$ entries containing the position of errors applied to the physical qubits for any given episode. This state is hidden from A and it is used to generate the state space \mathcal{S} , comprised of the error syndrome of all stabilisers \mathcal{P} of the code, in this case a set of $d \times d$ matrices representing the position of each stabilizer and its corresponding error syndrome. This situation can be regarded as an example of a partially observable Markov decision process [59].

The agents actions consist of single qubit bit flip operations. In principle, we can allow the agent to act on any of the $2d^2$ qubits. However, it is inconvenient to let the agent perform bit-flip operations to qubits which do not have an adjacent violated syndrome. Such qubits are not candidates of having produced the syndrome errors, and thus should not be altered. Therefore, for a given state s , i.e., a given error syndrome, only a subset of all possible actions a (single qubit bit-flips) should be allowed and these actions are different for different syndrome errors. As the neural network needs to have a fixed output dimension, we need to make adjustments in order to appropriately accommodate the restrictions on the agents possible actions. One possibility would be to calculate the q -values for all $2d^2$ qubits, and allow the agent to perform only the valid actions but this results in large training times for the agent. Whilst this strategy does work it is extremely inefficient, particularly for large lattice dimensions.

In order to speed up the learning stage, a convenient representation of the errors must be given to the neural network. By exploiting the boundary conditions of the torus Andreasson *et al.* provide one such representation in terms of so-called *perspectives* shown in Fig. 5 [27]. The syndrome error of any stabilizer can be represented as an arbitrary plaquette at the center of the torus. For each syndrome we can generate a set of matrices—the perspectives B_i —each of them having a different defect at its center while keeping the relative position of other defects fixed. The input to the neural network are the perspectives B_i , for which the neural network provides the q -value for each of the four possible actions; X corrections on the qubits adjacent to the vertex in question. In other words, instead of inputting one single matrix containing the syndrome errors, N matrices are given as an input, N being the number of syndrome errors. In this way, the output of the neural network is reduced from $2d^2$ to $4N$, allowing for a more efficient and stable training phase.

The agent continues to perform actions until the *terminal state* of the environment is reached: all syndrome measurements have outcome +1. As we compute the actions A performs on the hidden state of the code along the way we can evaluate the number of non-trivial horizontal or vertical loops around the torus. If an even number of such loops is found, no logical errors have occurred and the agent is rewarded a nominal reward

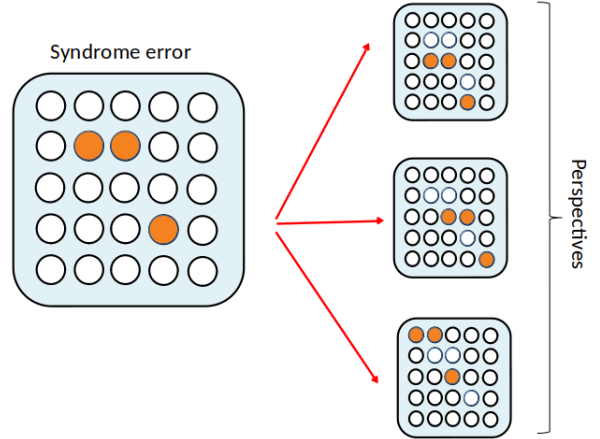


FIG. 5. Example of the representation of errors given to the neural network. Given a syndrome with N errors, we produce N perspectives by locating a defect to the central plaquette, while keeping the relative position of the other defects fixed. The set of perspectives are given to the neural network as an input.

of $r = +1000$ [60]. Else, the agent’s reward is $r = 0$. In [27], a RL decoder for the same task was designed using similar techniques as ours. There the agent was penalised with $r = -1$ for every iteration, so that the optimal strategy would be to correct the error syndrome with the minimum number of operations. We shall refer to the decoder of [27] as a *minimum action decoder*, or MAD for short, and will compare this reward scheme with ours.

We train the agent using the DQL algorithm, until the parameters of the convolutional neural network stabilize. In order to give the agent more freedom to explore the large policy space during training we use an ϵ -greedy strategy for Q -learning; with probability $1 - \epsilon$ the agent selects the action with the highest value of the current q -function, whereas with probability ϵ the agent performs an action at random. Furthermore, we vary the value of ϵ during training, linearly decreasing it to the minimum value of $\epsilon = 0.1$. Moreover, we also train the agent with an initially low probability of bit flip errors so that A learns to correct properly, linearly increasing the occurrence of errors near-to and beyond the 11% threshold of the code.

Neural Network architecture and training parameters

In this section we provide the technical details used to design the neural network and training phase of the agent. The neural network consists of some convolutional layers, a set of fully connected layers and an output layer with four values. Each output corresponds to applying an action to one of the qubits adjacent to the input plaquette. The algorithm we im-

plement is given in Table 1. The network is trained by adjusting the hyper parameters θ_i at iteration i such that the error between the optimal target values $r + \gamma \max_{a'} q^*(s', a')$ and the approximated target values $y_i = r + \gamma \max_{a'} q(s', a', \theta_i)$, calculated using the Q-network, is reduced. Training consists in decreasing this loss function via stochastic gradient descend, until the Q-network produces precise values of the q-function.

The fact that the approximate target values y_i depend on the network parameters produces instabilities in the training process, and could lead to divergence of the network weights. To that end we use a separate network for generating the targets $y_i = r + \gamma \max_{a'} \hat{q}(s', a', \theta_i)$ in the Q-learning update. More precisely, for every K updates we clone the *active* Q-network (the one used to select the best action in each state) to obtain a *target* Q-network, which is used to generate the targets y_j for the following K updates. Table I shows the parameters used for the neural network architecture. Table II shows the common hyper-parameters used for the agents, whilst table III shows the hyper-parameters which were different.

Algorithm 1 Deep Q-learning

- 1: **procedure** INITIALIZATION:
 - 2: Initialize replay memory D
 - 3: Initialize active Q-network q with random weights θ
 - 4: Initialize target Q-network \hat{q} with random weights θ^-
 - 5: **for** $t=1 \dots M$ **do**
 - 6: With probability ϵ select a random action a_t
 - 7: Otherwise select action $a_t = \operatorname{argmax}_{a'} q(s', a, \theta)$
 - 8: Execute action a_t , receive reward r_t and next state s_{t+1}
 - 9: Store experience $e_t = (s_t, a_t, r_t, s_{t+1})$ in memory D
 - 10: Select a random sample $\{e_{i_1}, \dots, e_{i_j}\}$ from D
 - 11: **for** every experience in sample **do**
 - 12: Calculate target values $y_i = r_i + \gamma \max_{a'} \hat{q}(s_i, a_i, \theta^-)$, with $\hat{q}(s_i, a_i, \theta^-) = 0$ if s_i is a terminal state
 - 13: Perform a gradient descent step on $(y_i - q(s_i, a_i, \theta))$ with respect to the network parameters θ :
 - 14:
$$\Delta\theta = \alpha(r_i + \gamma \max_{a'} \hat{q}(s_{i+1}, a', \theta^-) - q(s_i, a_i, \theta)) \nabla_{\theta} q(s_i, a_i, \theta)$$
 - 15: **end for**
 - 16: Every K iterations reset $\hat{q} = q$
 - 17: **end for**
 - 18: **end procedure**
-

Results

We now present our results on RL decoders for uncorrelated noise on the toric code. Agents were trained on grids of dimensions, $d = 3, 5, 7$ and 9 . After training, we evaluated the decoders performance for different error probabilities p . We define the logical success probability as the proportion of syndromes decoded successfully. As for uncorrelated errors the MWPM algorithm is near-optimal, we also compare the RL agent's performance with MWPM.

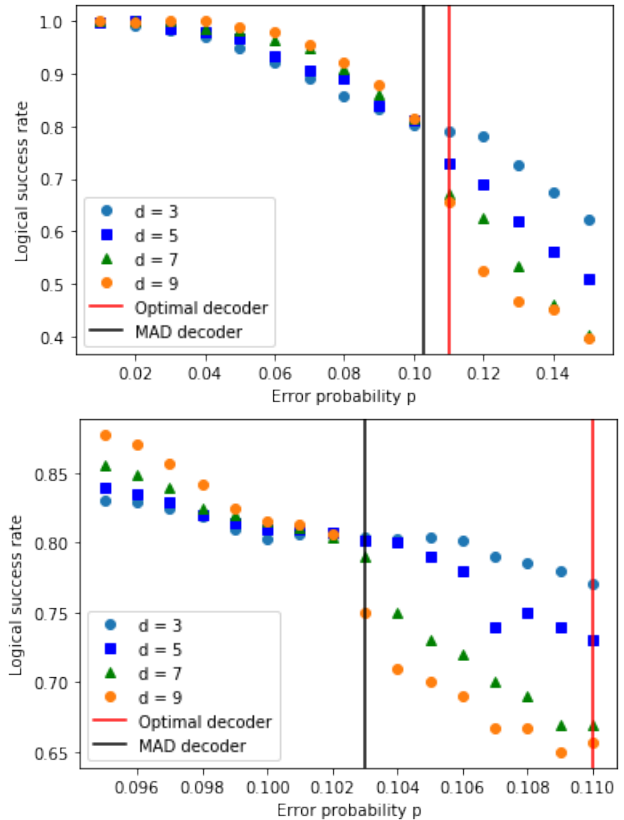


FIG. 6. Logical success probability as a function of error probability p for agents trained in different lattice dimensions $d = 3, 5, 7, 9$. The values of p range from $0.01 - 0.15$ (top) and from $0.095 - 0.11$ (bottom). All agents were trained with error probability $p = 0.10$. Thresholds for the optimal decoder and the MAD are shown as red and grey vertical bars, respectively.

Fig. 6 shows the logical success probability as a function of the error probability p for several lattice sizes. For $p \leq 0.10$ the performance of the RL agent improves with the dimension d , of the lattice. When the error probability p is low, the probability of successful decoding increases with the dimension of the lattice, whereas for p high the opposite effect occurs. The turning point between these two behaviors is called the *code threshold*. The code threshold for these agents falls between $p = 0.102$ and $p = 0.103$, similar to those obtained in [27]. We also tested decoders which were trained

Type	Size
Input layer	$d \times d$
Convolutional layer	512 filters, 3×3 size, 2×2 stride
Convolutional layer	256 filters, 3×3 size, 2×2 stride
Convolutional layer	256 filters, 3×3 size, 2×2 stride
Fully-connected layer	256 neurons
Fully-connected layer	128 neurons
Fully-connected layer	64 neurons
Fully-connected layer	32 neurons
Output layer	4 outputs

TABLE I. Summary of the deep neural network architecture.

Agent	ϵ initial	ϵ final	# iterations	p initial	p final	# iterations with p final	γ
$d = 3$	0.75	0.08	1000	0.01	0.10	300	0.9
$d = 5$	0.75	0.08	2500	0.01	0.10	1000	0.95
$d = 7$	0.75	0.08	6000	0.01	0.10	2000	0.95
$d = 9$	0.5	0.1	8000	0.01	0.10	3500	0.95

TABLE III. Summary of the different hyper-parameters for each agent.

with error probabilities higher than the code threshold $p = 0.15$, and $p = 0.2$. We noticed a slight increase in performance in the former case whilst in the latter decoders performed significantly worse.

A more direct comparison between our decoder and the one of [27] is shown in Fig. 7. We trained an agent according to the reward system of [27], and compared the episode length distribution for both agents. For $d = 5$ both agents seem to have very similar episode length distributions meaning that an agent trained based on success/failure reward learnt that, in general, the best strategy is indeed to nullify the error syndrome as quickly as possible even though it was not explicitly told so. For $d = 3$, the episode length distributions are more distinct. By and large the agent adopts a decoding strategy requiring the least amount of corrections but occasionally slightly more steps are required.

Our results indicate that it is not necessary to train agents based on minimizing their number of actions and that the natural choice of reward based on correct decoding is capable of learning the best policy, even yielding slight improvements in performance. A comparison of the efficiencies of the two decoders is shown in Fig. 8. For $d = 5$ both agents have very similar success probability. However, for $d = 3$, the agent trained with success/failure rewards outperforms the one of [27] indicating that the different policy adopted by the success/failure agent is in fact beneficial for correct decoding of the code.

Finally, Table IV shows the training times required for the various lattice sizes considered. All training was performed using a single desktop computer.

Parameter	Value
Input layer	$d \times d$
Batch size	32
Maximum training steps	1000
Memory buffer size	3000000
Target update iterations	500
Learning rate	0.0001
β_{a_1}	0.9
β_{a_2}	0.999
Optimizer	Adam
Rewards	+1000 if success 0 if failure

TABLE II. Summary of the common hyper-parameters for all agents.

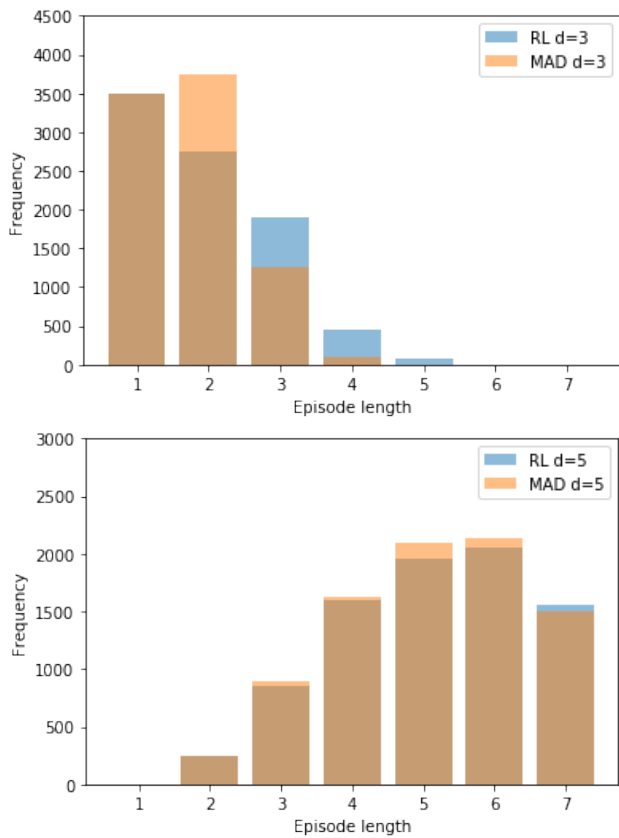


FIG. 7. Episode length distribution for agents trained based on minimizing the number of actions and agents trained based on rewarding solely on successful decoding for $d = 3$ (left) and $d = 5$ (right).

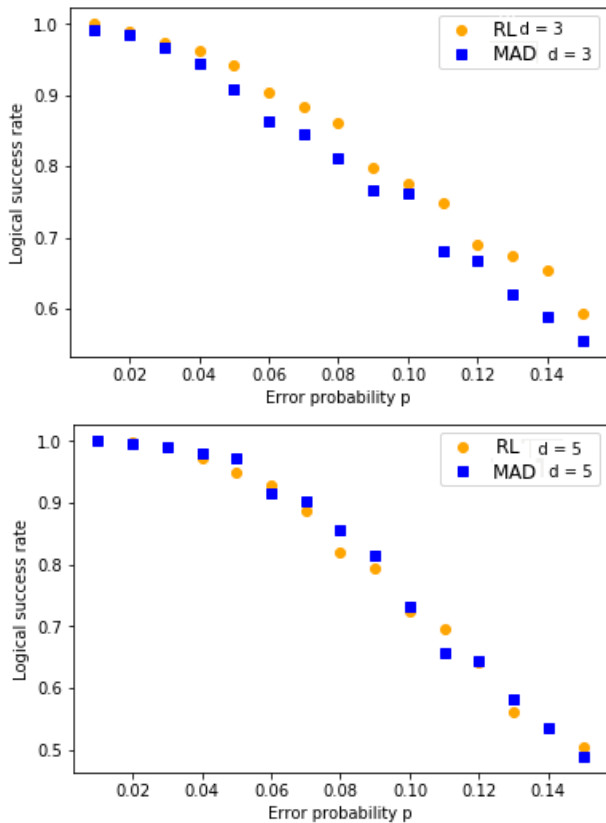


FIG. 8. Logical success probability as a function of error probability p for agents trained with success/failure rewards and rewards based on the number of actions taken for $d = 3$ (left) and $d = 5$ (right).

Lattice dimension	d=3	d=5	d=7	d=9
Training time (hrs)	0.33	5	12	32

TABLE IV. Training time for each Reinforcement Learning model.

V. SUMMARY AND CONCLUSIONS

In this work we used deep Q-learning to train an agent using reinforcement learning in order to decode uncorrelated errors on a toric code. We showed that agents can be trained based on whether or not correct decoding of the errors has been performed and showed that such decoders achieve near optimal performance. Our agents are more versatile as compared to those trained based on minimising the number of actions taken, which leads to slightly improved performance on smaller lattices. Moreover, by comparing the episode length distributions between the two different types of agents we observe that indeed policies based on performing the minimum number of actions seem to form the most efficient decoders.

We believe that our model-free scheme of choosing rewards based solely on the success/failure of the decoding procedure is more versatile and can be used to design decoders for other TECC, such as surface codes, or the Kagome lattice, as well as for more general noise models. We expect that our approach is able to address error correction for correlated noise for which minimum action decoding methods are unsuitable. Work along this line is currently under consideration.

ACKNOWLEDGEMENTS

The authors acknowledge support from Spanish MINECO reference FIS2016-80681-P (with the support of AEI/FEDER,EU); the Generalitat de Catalunya, project CIRIT 2017-SGR-1127 and the Baidu-UAB collaborative project 'Learning of Quantum Hidden Markov Models'.

REFERENCES

- [1] A. Galindo and M. A. Martín-Delgado, Rev. Mod. Phys. **74**, 347 (2002).
- [2] I. M. Georgescu, S. Ashhab, and F. Nori, Rev. Mod. Phys. **86**, 153 (2014).
- [3] N. Gisin and R. Thew, Nat. Photonics **1**, 165 (2007).
- [4] V. Giovannetti, S. Lloyd, and L. Maccone, Nat. Photonics **5**, 222 (2011).
- [5] C. L. Degen, F. Reinhard, and P. Cappellaro, Rev. Mod. Phys. **89**, 035002 (2017).
- [6] D. Gottesman, in *Quantum information science and its contributions to mathematics, Proceedings of Symposia in Applied Mathematics*, Vol. 68 (2010) pp. 13–58.
- [7] B. M. Terhal, Rev. Mod. Phys. **87**, 307 (2015).
- [8] E. T. Campbell, B. M. Terhal, and C. Vuillot, Nature **549**, 172 (2017).
- [9] S. B. Bravyi and A. Kitaev, arXiv preprint quant-ph: 9811052 (1998).
- [10] H. Bombín, arXiv preprint quant-ph: 1311.0277 (2013).
- [11] M. Herold, E. T. Campbell, J. Eisert, and M. J. Kastoryano, npj Quantum information **1**, 15010 (2015).
- [12] M. Herold, M. J. Kastoryano, E. T. Campbell, and J. Eisert, New J. Phys. **19**, 063012 (2017).
- [13] N. Lang and H. P. Büchler, SciPost Phys. **4**, 007 (2018).
- [14] A. Kubica and J. Preskill, Phys. Rev. Lett. **123**, 020501 (2019).
- [15] G. Duclos-Cianci and D. Poulin, in *2010 IEEE Information Theory Workshop (IEEE, 2010)* pp. 1–5.
- [16] G. Duclos-Cianci and D. Poulin, Phys. Rev. Lett. **104**, 050504 (2010).
- [17] G. Torlai and R. G. Melko, Phys. Rev. Lett. **119**, 030501 (2017).
- [18] S. Varsamopoulos, B. Criger, and K. Bertels, Quantum Science and Technology **3**, 015004 (2017).
- [19] S. Krastanov and L. Jiang, Sci Rep-UK **7**, 11003 (2017).

- [20] P. Baireuther, T. E. O'Brien, B. Tarasinski, and C. W. Beenakker, *Quantum* **2**, 48 (2018).
- [21] T. Fösel, P. Tighineanu, T. Weiss, and F. Marquardt, *Phys. Rev. X* **8**, 031084 (2018).
- [22] C. Chamberland and P. Ronagh, *Quantum Science and Technology* **3**, 044002 (2018).
- [23] R. Sweke, M. S. Kesselring, E. P. van Nieuwenburg, and J. Eisert, arXiv preprint arXiv:1810.07207 (2018).
- [24] Y.-H. Liu and D. Poulin, *Phys. Rev. Lett.* **122**, 200501 (2019).
- [25] S. Varsamopoulos, K. Bertels, and C. G. Almudever, arXiv preprint arXiv:1901.10847 (2019).
- [26] N. Maskara, A. Kubica, and T. Jochym-O'Connor, *Phys. Rev. A* **99**, 052351 (2019).
- [27] P. Andreasson, J. Johansson, S. Liljestrand, and M. Granath, *Quantum* **3**, 183 (2019).
- [28] J. Edmonds, *Can. J. Math.* **17**, 449467 (1965).
- [29] H. Poulsen Nautrup, N. Delfosse, V. Dunjko, H. J. Briegel, and N. Friis, *Quantum* **3**, 215 (2019).
- [30] A. Valenti, E. van Nieuwenburg, S. Huber, and E. Greplova, *Phys. Rev. Research* **1**, 033092 (2019).
- [31] D. A. Lidar and T. A. Brun, *Quantum error correction* (Cambridge university press, 2013).
- [32] D. Gottesman, *Stabilizer Codes and Quantum Error Correction*, Ph.D. thesis, California Institute of Technology (1997).
- [33] D. Poulin, *Phys. Rev. Lett.* **95**, 230504 (2005).
- [34] X.-C. Yao, T.-X. Wang, H.-Z. Chen, W.-B. Gao, A. G. Fowler, R. Raussendorf, Z.-B. Chen, N.-L. Liu, C.-Y. Lu, Y.-J. Deng, *et al.*, *Nature* **482**, 489 (2012).
- [35] D. Nigg, M. Mueller, E. A. Martinez, P. Schindler, M. Hennrich, T. Monz, M. A. Martin-Delgado, and R. Blatt, *Science* **345**, 302 (2014).
- [36] C. D. Hill, E. Peretz, S. J. Hile, M. G. House, M. Fuechsle, S. Rogge, M. Y. Simmons, and L. C. Hollenberg, *Science Advances* **1**, e1500707 (2015).
- [37] A. D. Córcoles, E. Magesan, S. J. Srinivasan, A. W. Cross, M. Steffen, J. M. Gambetta, and J. M. Chow, *Nat. Commun.* **6**, 6979 (2015).
- [38] J. Kelly, R. Barends, A. G. Fowler, A. Megrant, E. Jeffrey, T. C. White, D. Sank, J. Y. Mutus, B. Campbell, Y. Chen, *et al.*, *Nature* **519**, 66 (2015).
- [39] D. Riste, S. Poletto, M.-Z. Huang, A. Bruno, V. Vesterinen, O.-P. Saira, and L. DiCarlo, *Nat. Commun.* **6**, 6983 (2015).
- [40] M. Takita, A. D. Córcoles, E. Magesan, B. Abdo, M. Brink, A. Cross, J. M. Chow, and J. M. Gambetta, *Phys. Rev. Lett.* **117**, 210505 (2016).
- [41] E. Dennis, A. Kitaev, A. Landahl, and J. Preskill, *J. Math. Phys.* **43**, 4452 (2002).
- [42] H. N. Gabow, *JACM* **23**, 221 (1976).
- [43] W. Cook and A. Rohe, *INFORMS J. Comput.* **11**, 138 (1999).
- [44] D. Browne, "Lectures on topological codes and quantum computation," (2014), (Accessed on 30/10/2019).
- [45] R. S. Sutton, A. G. Barto, *et al.*, *Introduction to reinforcement learning*, Vol. 2 (MIT press Cambridge, 1998).
- [46] D. Silver, A. Huang, C. J. Maddison, A. Guez, L. Sifre, G. Van Den Driessche, J. Schrittwieser, I. Antonoglou, V. Panneershelvam, M. Lanctot, *et al.*, *Nature* **529**, 484 (2016).
- [47] G. B. Orr and K.-R. Müller, *Neural networks: tricks of the trade* (Springer, 2003).
- [48] S. Ramos, S. Gehrig, P. Pinggera, U. Franke, and C. Rother, in *2017 IEEE Intelligent Vehicles Symposium (IV)* (IEEE, 2017) pp. 1025–1032.
- [49] R. Brunelli and T. Poggio, *IEEE transactions on pattern analysis and machine intelligence* **15**, 1042 (1993).
- [50] Note that we can always consider finite sequences by introducing a terminal state for the environment indicating that the task is completed.
- [51] R. Bellman, *Indiana Univ. Math. J.* **6**, 679 (1957).
- [52] The use of a discount rate is particularly useful for dealing with continuous interactions between agent and environment, i.e., for continuous sequences.
- [53] R. Bellman, *Science* **153**, 34 (1966).
- [54] M. L. Puterman, *Markov decision processes: discrete stochastic dynamic programming* (John Wiley & Sons, 2014).
- [55] N. Kalchbrenner, E. Grefenstette, and P. Blunsom, arXiv preprint arXiv:1404.2188 (2014).
- [56] V. Mnih, K. Kavukcuoglu, D. Silver, A. A. Rusu, J. Veness, M. G. Bellemare, A. Graves, M. Riedmiller, A. K. Fidjeland, G. Ostrovski, *et al.*, *Nature* **518**, 529 (2015).
- [57] V. Mnih, K. Kavukcuoglu, D. Silver, A. Graves, I. Antonoglou, D. Wierstra, and M. Riedmiller, arXiv preprint arXiv:1312.5602 (2013).
- [58] T. Simonini, "Improvements in Deep Q Learning: Dueling Double DQN, Prioritized Experience Replay, and fixed Q-targets," (2018).
- [59] J. Barry, D. T. Barry, and S. Aaronson, *Physical Review A* **90**, 032311 (2014).
- [60] The value of the reward is chosen so as to speed-up the training process.